

BIRA: A Spherical Bistatic Reflectivity Measurement System

Carsten Andrich¹, Tobias F. Nowack, Alexander Ihlow², Sebastian Giehl², Maximilian Engelhardt¹,
Gerd Sommerkorn¹, Andreas Schwind¹, Willi Hofmann, Christian Bornkessel,
Reiner S. Thomä¹, *Life Fellow, IEEE*, Matthias A. Hein¹, *Senior Member, IEEE*

Abstract—The upcoming 6G mobile communication standard will offer a revolutionary new feature: Integrated sensing and communication (ISAC) reuses mobile communication signals to realize multi-static radar for various applications including localization. Consequently, applied ISAC propagation research necessitates to evolve from classical monostatic radar cross section (RCS) measurement of static targets on to bistatic radar reflectivity characterization of dynamic objects. Here, we introduce our “Bistatic Radar” (BIRA) and antenna measurement facility for bistatic spherical positioning with sub-millimeter accuracy on a diameter of up to 7 m and with almost continuous frequency coverage from 0.7 up to 260 GHz. Currently, BIRA is the only bistatic measurement facility capable of unrestricted ISAC research: In addition to vector network analysis, BIRA employs advanced wideband transceiver technology with an instantaneous bandwidth of up to 4 GHz. These transceivers grant BIRA the unique ability to characterize dynamic targets in both Doppler and range, while also significantly accelerating RCS measurements of static objects.

Index Terms—Radar reflectivity, radar cross section, bistatic radar measurement, millimeter wave antenna testing, spherical gantry positioner, anechoic chamber, wideband transceiver, integrated sensing and communication.

I. INTRODUCTION

Applied microwave propagation research is indispensable for automated and connected mobility and its vital need for reliable communication and accurate sensing. In this regard, the future mobile communication standard 6G will include a revolutionary new feature: Integrated sensing and communication (ISAC). In contrast to traditional, monostatic Radar systems, ISAC is inherently bistatic, therefore necessitating bistatic measurement infrastructure for experimental research. Additionally, the microwave spectrum envisioned for 6G requires antenna characterization in the sub-THz frequency range.

The Thuringian Center of Innovation in Mobility (ThIMo) in its core competence “wireless and information technology” has been conducting leading research of wireless transmission

The research was funded by the Federal State of Thuringia, Germany, and the European Social Fund (ESF) under grants 2017 FGI 0007 (project “BiRa”), 2021 FGI 0007 (project “Kreatör”), and 2023 IZN 0005 (project “FoDiMo”).

All authors are with the Thuringian Center of Innovation in Mobility, Ilmenau, Germany.

Carsten Andrich, Alexander Ihlow, Sebastian Giehl, Maximilian Engelhardt, Gerd Sommerkorn, and Reiner S. Thomä are also with the Institute of Information Technology, Technische Universität Ilmenau, Ilmenau, Germany.

Andreas Schwind, Willi Hofmann, Christian Bornkessel, and Matthias A. Hein are also with the RF and Microwave Research Group, Technische Universität Ilmenau, Ilmenau, Germany.

related to road and rail traffic and drones, based on its automotive antenna facility Virtual Road – Simulation and Test Area (VISTA) since 2014. VISTA comprises an anechoic chamber, a turntable positioner with 6.5 m diameter, and an antenna measurement arch [1]. Over the last decade, VISTA has enabled diverse and novel contributions on, e.g., vehicle-in-the-loop virtual drive testing for mobile communication systems [2], performance evaluation of automotive antennas in their installed state, including phaseless antenna measurements [3], automotive radar testing [4], and realistic emulation of global navigation satellite system (GNSS) signals [5]. Although we have utilized VISTA for static [6] and dynamic [7] ISAC measurements, for lack of suitable mechanical positioning infrastructure, the respective bistatic geometries were restricted to the horizontal plane. This limitation has motivated us to upgrade VISTA from an antenna measurement chamber to the universal bistatic measurement facility “Bistatic Radar” (BIRA) with eight mechanical degrees of freedom. Its mechanical and spectral capabilities qualify BIRA for comprehensive 6G research, e.g., antenna measurement up to sub-THz frequencies and dynamic radar reflectivity characterization for ISAC.

The paper is structured as follows: Sec. II provides a comparison with state-of-the-art bistatic measurement facilities. Sec. III describes the mechanical aspects of the BIRA system and Sec. IV explains its measurement transceivers and interchangeable microwave probe modules. Then, Sec. V illustrates the associated software suite comprising a digital twin and a generic application programming interface (API) and abstraction layer. Finally, Sec. VI summarizes this paper.

II. STATE OF THE ART

Only a few measurement facilities are known to enable measurements of the bistatic reflectivity of extended targets. Those found in the literature will be introduced in the following. To facilitate a comparison by features, their capabilities are contrasted with those of BIRA in Table I. The transmitter (Tx) and receiver (Rx) positioner characteristics (azimuth and co-elevation) are given within the respective machine coordinate system. Together with the DUT rotation (turntable), the mechanical degrees of freedom of the positioners result in a set of reachable bistatic angles from the DUT perspective.

1.) The bistatic anechoic chamber (BIANCHA) of the *National Institute for Aerospace and Technology* (INTA) in Torrejón de Ardoz, Spain, consists of a turntable and two gantry arms, providing four degrees of freedom [8], [9].

TABLE I
COMPARISON OF BIRA AND STATE-OF-THE-ART BISTATIC MEASUREMENT FACILITIES FROM LITERATURE.

	presented here	bistatic measurement facilities described in literature				
	BIRA @TU Ilmenau, DE	BIANCHI @INTA, ES	CACTUS @CESTA, FR	BABI @ONERA, FR	EMSL @Ispra, IT	LAMP @DASA, CN
inauguration	2023	2010	<2007	1990s	1992	2019
principle	two gantry arm positioners	two elevated scanning arms	two slides on one shared circular azimuth rail	two slides on one shared circular azimuth rail	two slides on one shared elevation arc orbit	two slides on one shared elevation arc orbit
target distance	≤ 3.5 m; w/ RF probe ≈ 3 m	1.74 m	a few m	5.5 m	10 m	9.3 m
# mech. DoF*	8	4	2	2	3	3
DUT \odot	\checkmark turntable $360^\circ \varnothing 6.5$ m	\checkmark turntable $360^\circ \varnothing < 1$ m	– pillar	– mast, adjustable height	\checkmark turntable 360° on rails	\checkmark turntable 360° on rails
Tx azimuth	$\checkmark -118^\circ \dots 66^\circ$	– (fixed)	$\checkmark 0^\circ \dots 180^\circ$	$\checkmark 0^\circ \dots 190^\circ$	– (fixed)	– (fixed)
Rx azimuth	– (fixed)	$\checkmark -200^\circ \dots 200^\circ$	$\checkmark 0^\circ \dots 180^\circ$	$\checkmark 0^\circ \dots 190^\circ$	– (fixed)	– (fixed)
Tx co-elev.	$\checkmark -114^\circ \dots 114^\circ$	$\checkmark -100^\circ \dots 100^\circ$	– (fixed, 90°)	– (manually, $70^\circ \dots 90^\circ$)	$\checkmark -115^\circ \dots 115^\circ$	$\checkmark -90^\circ \dots 90^\circ$
Rx co-elev.	$\checkmark -115^\circ \dots 115^\circ$	$\checkmark -100^\circ \dots 100^\circ$	– (fixed, 90°)	– (manually, $70^\circ \dots 90^\circ$)	$\checkmark -115^\circ \dots 115^\circ$	$\checkmark -90^\circ \dots 90^\circ$
Tx polariz.	$\checkmark -10^\circ \dots 188^\circ$	–	–	–	–	–
Rx polariz.	$\checkmark -10^\circ \dots 188^\circ$	–	–	–	–	–
Tx radial	$\checkmark 3.44$ m ± 6 cm	–	–	–	–	–
Rx radial	$\checkmark 3.44$ m ± 6 cm	–	–	–	–	–
bistatic angles [‡]	more than hemisphere	more than hemisphere	partial azimuth	partial azimuth	partial hemisphere	partial hemisphere
φ_i	$0^\circ \dots 360^\circ$	$0^\circ \dots 360^\circ$	$0^\circ \dots 180^\circ$	$0^\circ \dots 190^\circ$	$0^\circ \dots 360^\circ$	$0^\circ \dots 360^\circ$
φ_o	$0^\circ \dots 360^\circ$	$0^\circ \dots 360^\circ$	few $^\circ \dots 180^\circ$	$4^\circ \dots 190^\circ$	0° or 180°	0° or 180°
θ_i	$0^\circ \dots 114^\circ$	$0^\circ \dots 100^\circ$	90° (fixed)	$70^\circ \dots 90^\circ$ (manually)	$0^\circ \dots 115^\circ$	$0^\circ \dots 90^\circ$
θ_o	$0^\circ \dots 115^\circ$	$0^\circ \dots 100^\circ$	90° (fixed)	$70^\circ \dots 90^\circ$ (manually)	$0^\circ \dots 115^\circ$	$0^\circ \dots 90^\circ$
measurement instrumentation	VNA (for static DUTs); wideband SDR transceivers (resolve Doppler dynamics)	VNA	VNA	VNA	VNA	VNA
frequency range	0.7...20 GHz, with conversion: ≤ 260 GHz	0.8...40 GHz	1...18 GHz	0.5...40 GHz	0.7...50 GHz	0.8...20 GHz
probes	arbitrary, $\approx 50 \times 30 \times 30$ cm, ≤ 20 kg (antennas, frequency converters, transceivers, sensors, e.g., Lidar, ToF, ...)	antennas	antennas	antennas	antennas	antennas
additional payload on positioners	mounting plate 38×17 cm for ≤ 35 kg payload (e.g., transceivers)					
reference	[this paper]	[8]–[10]	[11]	[12]	[13], [14]	[15], [16]

* Number of mechanical degrees of freedom. Mechanical parameters are given within the respective machine coordinate system. It differs from the bistatic angles, which are relative to the DUT. 0° co-elevation locates the probe in the zenith.

[‡] φ_i, θ_i : illumination azimuth and co-elevation angle; φ_o, θ_o : observation angles. All coordinates are relative to the device under test (DUT), which is located at the origin of the spherical coordinate system. The x-y-plane is aligned with ground and the z-axis points towards the zenith. Co-elevation angle θ is defined down from the zenith. Note that the set of reachable azimuth angles φ_i, φ_o may also incorporate a DUT rotation with the turntable.

2.) In the CACTUS measurement facility at the *centre d'études scientifiques et techniques d'Aquitaine* (Cesta) in France, two pedestals with elevated antennas can move along a circular rail (on the floor), providing two degrees of freedom [11].

3.) Similarly, in the BABI measurement chamber of the *office national d'études et de recherches aérospatiales* (Onera) in France, the antennas slide on an elevated circular rail [12].

4.) The European Microwave Signature Laboratory (EMSL), located in Ispra, Italy, contains an elevation arch with two sliding antennas and a 360° turntable DUT positioner [13], [14].

5.) The Laboratory of Target Microwave Properties (LAMP), located in Deqing, Zhejiang, China is a facility similar to EMSL. The chamber structure itself with two sliding antennas on an elevation arch and the DUT placement onto a turntable on rails is comparable to EMSL [15], [16].

Only BIANCHA and BIRA enable unrestricted, bistatic, spherical positioning, i.e., setting illumination azimuth angle φ_i and co-elevation angle θ_i independently of observation azimuth angle φ_o and co-elevation angle θ_o , which we consider mandatory for bistatic radar reflectivity and antenna measurement research. Exclusively BIRA is large enough for target objects up to the size of a passenger car. Regarding the measurement instrumentation, all facilities use vector

network analyzers (VNAs). In contrast, BIRA also features software-defined radio (SDR) transceivers for Doppler and range resolved measurement of time-variant targets, which are integral to ISAC research. Additionally, BIRA supports arbitrary probes and payloads that enable 6G-ready frequency coverage up to 260 GHz through converters. Owing to its unique capabilities, BIRA is currently the only published bistatic measurement facility capable of performing unrestricted ISAC research.

III. CONCEPT AND MECHANICAL PROPERTIES

The Virtual Road – Simulation and Test Area (VISTA) depicted in Fig. 1 provides the ideal prerequisites for bistatic reflectivity and antenna measurements of target objects up to the size of a passenger car. VISTA comprises a shielded, anechoic chamber with $13 \text{ m} \times 9 \text{ m} \times 7.5 \text{ m}$ of usable interior volume, a turntable with 6.5 m diameter for loads up to 3000 kg, and a permanently installed SG 3000F multi-probe antenna measurement arch for frequencies from 70 MHz up to 6 GHz [1].

The immovable measurement arch necessitates two significant constraints for the installation of our bistatic positioning system BIRA: It must fit within the inner diameter of the arch and, more importantly, it must be removable and re-installable to enable unobstructed use of the multi-probe



Fig. 1. Virtual Road – Simulation and Test Area (VISTA) at the Thuringian Center of Innovation in Mobility (ThIMo), without the BIRA bistatic measurement system installed. A passenger car is placed on the turntable (hidden under pyramidal absorbers) and elevated to the focal point of the antenna arch, enabling spherical measurements with two degrees of freedom [1].

system. Assembly duration should be no more than a single day and repeated re-installation must not degrade mechanical accuracy. The contractor commissioned with the development and installation of BIRA was Celestia Mechantronic Test Systems (C-MTS).

BIRA comprises two modular gantry positioners (see Fig. 2) enabling almost arbitrary positioning of two probes on the same sphere with a radius of approximately 3 m and its origin in the focal point 2.27 m above the turntable in the plane of the Microwave Vision Group (MVG) arch. Both gantries can be installed independently, enabling single gantry operation. The gantry mounting plates are located below the metallic false floor. When not installed, the respective cutouts in the false floor are covered by metal plates with minimal clearances. Each gantry is composed of multiple modules that can be installed incrementally, with the first module fastened on the mounting plate. Precision positioning pins between the modules ensure repeat accuracy between assembly cycles.

Relying on the static gantry (see Fig. 2 (a)), the moving gantry and the turntable, BIRA has a total of eight degrees of freedom, separated into the following axes:

1) *Azimuth*: The moving gantry is mounted on a semi-circular rail around the focal point, enabling independent azimuth positioning (see Fig. 2 (f)). The static gantry's mounting plate is fixed directly to the building foundation. With respect to the DUT on the turntable, the azimuth positioning is realized by rotating the turntable.

2) *Elevation*: Both gantries implement spherical positioning on more than a hemisphere by means of rotating a raised boom in the shape of a flattened quarter circle (see Fig. 2 (i)). The boom's center of rotation is located in the horizontal plane of the focal point. Consequently, the probe at the boom tip always points radially towards the focal point. Note that due to this geometry the effective azimuth position of the probe is offset by $\pm 90^\circ$ relative to the center of rotation.

3) *Rotation/Polarization*: The gantry geometry inherently guarantees that the probe is not rotated around the radial axis

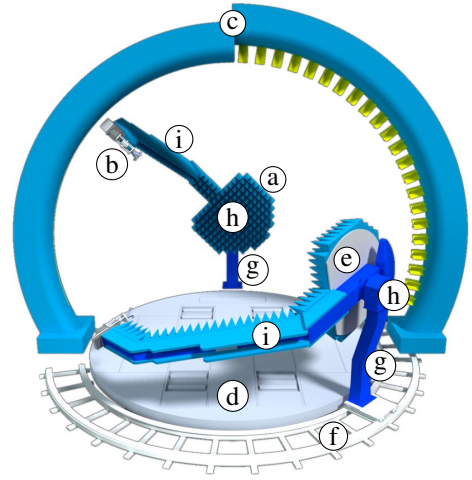


Fig. 2. 3D model of VISTA with both BIRA positioners installed. The static gantry elevation positioner (a) moves its probe (b) in the plane of the measurement arch (c). The static gantry does not move in azimuth, but instead the DUT rotates with the turntable (d). The moving gantry (e) is installed on a semi-circular rail (f), enabling azimuth and elevation positioning fully independently of the static gantry system. Pedestals (g) raise the center of rotation of both gantry arms (h) to 2.27 m above the floor. The flattened quarter circle booms (i) enable spherical positioning of two probes on significantly more than a hemisphere.

towards the focal point when moving in either azimuth or elevation. A noteworthy exception is the 180° inversion of the rotation angle when the elevation passes the zenith. For the purpose of intentionally rotating the probe, it is fixed to an electronic roll positioner at the tip of the boom (see Fig. 3). This enables, e.g., dual-polarized measurements with linearly polarized antennas (see Sec. IV-E).

4) *Radius*: The roll positioner itself is mounted on an electronic linear positioner aligned with the radial axis (see Fig. 3). This radial positioner can be used, e.g., to account for different probe lengths, to adjust for frequency-variant phase centers, or to augment nearfield to farfield transformation via the radial domain [17].

A dedicated laser tracking system was used to repeatedly measure the motion of all axes and to subsequently calibrate and adjust the system. These measurements have demonstrated a repeatable positioning accuracy for the azimuth axis of 0.02° (0.05° after reassembly) and for the elevation axes of 0.006° (0.02° after reassembly). The position-dependent elastic deformation from the weight of the positioners and the resulting position error are compensated automatically by the motor controller firmware based on the laser tracker calibration values.

The firmware is also responsible for mechanical safety: As the components of both positioners are located predominantly on the surface of the same sphere, collisions are physically possible. The firmware dynamically detects an imminent collision and prevents it by automatically enforcing an emergency stop, which is only the last out of several safety measures. See Sec. V for details on the remaining safety procedures.

The rotating gantry geometry of BIRA enables fully covering its surfaces facing the DUT with microwave absorbers.

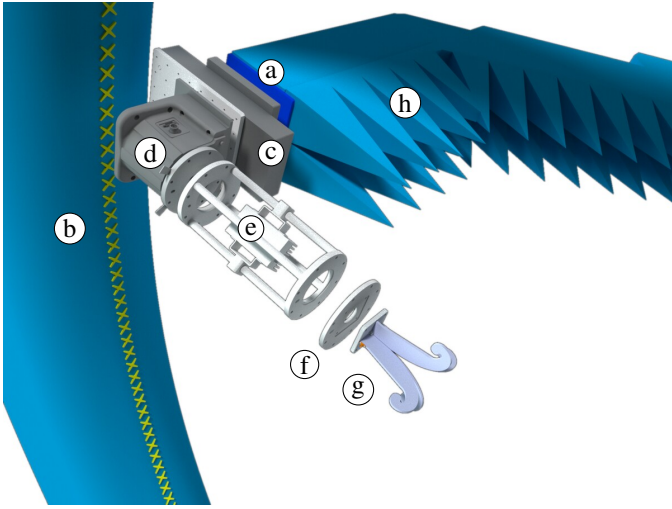


Fig. 3. Partially exploded assembly drawing of the static elevation positioner. Tip of the flattened quarter circle boom (a) in front of the left side of the multi-probe arch (b). Radial positioner (c) and polarization positioner (d) with universal probe flange. Exemplary probe (e) (microwave amplifier and polarization switch) with same flange as (d) on right-hand side. Exchangeable adapter disc (f) between universal probe flange and antenna (g). Microwave absorbers (h) are magnetically mounted to facilitate exchanging absorbers according to frequency range.

This is an advantage over other types of positioners, e.g., traveling trolleys (cf. Table I), which require an unobstructed rail for their motion. The absorbers are mounted magnetically to facilitate assembly and disassembly. Additionally, this enables the use of multiple sets of absorbers, each optimized for the respective frequency ranges of interest.

IV. UNIVERSAL PROBE AND TRANSCIVER SUPPORT

Versatility and modularity were primary design requirements for BIRA. These ensure future extensibility and frequency coverage up to the sub-THz range. Therefore, no measurement equipment is firmly integrated into the positioners. Probe flanges on the tips of the rotation positioners enable installation of arbitrary measurement probes (see Fig. 3). The backside of each gantry boom supports mounting additional payloads, also within generous size and mass constraints (see Table I). For each probe, BIRA provides up to 300 W of electrical power and general purpose input/output (GPIO) signals for electronic switching of gain and polarization. Additionally, each positioner is equipped with drag chains and empty conduits to enable the mechanically safe and straightforward installation of temporary wiring specific to the probe in use.

A. Monolithic VNA Transceivers

Bistatic radar reflectivity characterization necessitates signal transmission measurements with widely separated Tx and Rx antennas. Conventional measurement transceivers, e.g., VNAs, concentrate Tx and Rx ports into a single device. BIRA supports such monolithic transceivers with one integrated coaxial cable from each probe to directly adjacent connectors in the anechoic chamber. A central rotary joint in either elevation positioner incurs the mechanical limit of a single such cable per gantry.



Fig. 4. Non-converting microwave probes at tip of both gantry arm positioners: Tx and Rx amplifiers, RF switches for polarization, and RFspin QRH20E dual-polarized antennas surrounded by absorbers. This configuration is used for VNA measurements of static targets. See Table II for technical details.

The Tx cable length sums up to 30 m, because it passes through the azimuth rail drag chain of the moving positioner. The Rx cable spans only 17 m, as the azimuth position of the static gantry is fixed. These extensive cable lengths require both active and passive conditioning to enable frequency coverage from 0.5 to 26 GHz: Multiple wideband amplifiers compensate for high insertion loss, e.g., 60 dB at 26 GHz in the Tx path. Additionally, passive equalizers flatten the sloped frequency response of the cable to prevent non-linear distortion at lower frequencies, where electronic amplification would otherwise vastly exceed cable insertion loss.

We employ a Keysight N5222B VNA in combination with the coaxial cables described above, to measure the radar reflectivity of static targets or antennas under test. To enable time gating for the suppression of parasitic reflections, we typically rely on a 10 MHz step width, resulting in a 30 m spatial ambiguity limit.

B. Non-converting RF Probes for VNAs

When measuring with monolithic transceivers like VNAs, dual-polarized measurements require electronic switching in combination with the single cable connection between probe and VNA port. For our VNA applications up to 20 GHz, we rely on a pair of Tx/Rx probes that do not perform frequency conversion. Each probe implements amplification and polarization switching in the frequency range from 0.7 to 20 GHz. Both probes include a digital step attenuator for gain adjustment. Suitable quad-ridged dual-polarized antennas include a pair of Schwarzbeck CTIA0710 and a pair of RFspin QRH20E. See Fig. 4 for a picture of both radio frequency (RF) probes mounted on BIRA.

C. Software-defined Parallel Wideband Transceivers

Radar reflectivity measurements with VNAs typically require stepped positioning to avoid signal smear, because of

extended sweep times and – for BIRA – exacerbated by the need to sequentially switch polarizations. With bistatic radar reflectivity measurements encompassing at least four degrees of freedom, the constraint of stepped measurements results in long measurement times. Furthermore, VNAs are not suitable for radar reflectivity measurement of moving targets: Depending on carrier frequency and target motion speeds, even sweep times in the low millisecond range may be insufficient for Nyquist-compliant Doppler sampling. This constraint renders VNAs generally unsuitable for dynamic ISAC research.

For non-static measurement scenarios, we employ software-defined radio (SDR) transceivers with instantaneous bandwidths of 2 GHz or even 4 GHz in combination with IQ mixers or channel bonding [18]. These have already enabled unprecedented radar reflectivity and micro-Doppler signature measurements of moving targets [19], [20]. SDRs also significantly accelerate the bistatic measurement of static radar targets. Their negligible excitation signal periods enable continuous measurement while moving along a trajectory.

SDRs bear another advantage: We can deploy miniaturized and synchronized SDRs directly to each probe. This obviates the need for any actively conditioned, long-haul signal paths from the probes to a central monolithic transceiver. Implicitly, this also eliminates the previous limit of one single path: Multi-channel SDRs support parallel polarization measurements without Rx switching. The use of orthogonal excitation signals can even redundantize Tx switching.

We employ two *Xilinx RFSoc ZU47DR* direct RF sampling transceivers with a custom SDR firmware and software architecture [21]. Each transceiver offers eight analog-to-digital converter (ADC) channels and eight digital-to-analog converter (DAC) channels operating at sample rates up to 5 or 10 GSa/s, respectively. Both ADCs and DACs support sampling in the 2nd and 3rd Nyquist zones with a 6 GHz upper cutoff frequency. A centrally generated clock distributed optically via RF-over-fiber (RFoF) synchronizes both SDRs. Integrated 100 Gigabit Ethernet network interfaces stream samples to and from servers conveniently located outside of the anechoic chamber. Capable of arbitrary signal generation and sustained recording, the SDRs support a wide array of applications beyond bistatic transmissions measurements, e.g., signal and system emulation, hardware-in-the-loop testing, and generic 6G ISAC demonstrators [21].

D. Coaxial Quadrature Converters

The upper cutoff frequency of the SDR transceivers necessitates frequency converters for measurements above 6 GHz. Up to approximately 67 GHz, coaxial technology offers straightforward and affordable dual-polarized antennas and converters. In particular, quadrature mixers available for this frequency range provide frequency flexibility through inherent image suppression without external filters and intermediate frequency (IF) bandwidths of several GHz (cf. Table II). Their quadrature IF interface doubles the native instantaneous bandwidth of multi-port transceivers, achieving 4 GHz bandwidth in combination with our SDRs.

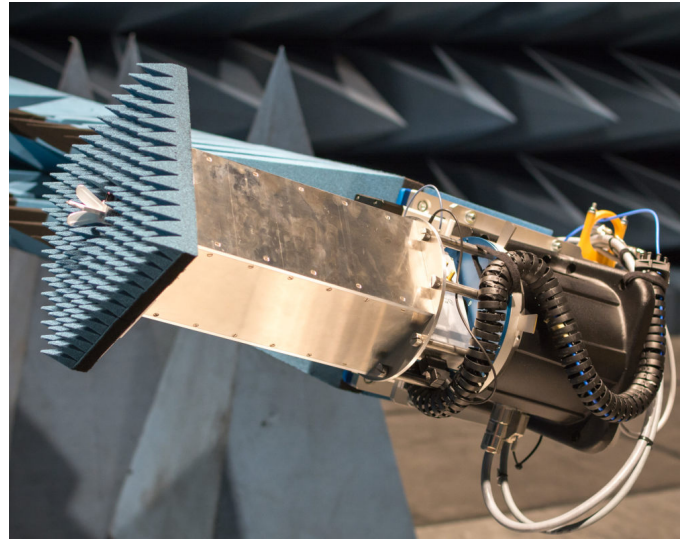


Fig. 5. Frequency converter with parallel microwave branches for both polarizations (4 IQ ports, entirely implemented in coaxial technology). These converters are designed primarily for Doppler-resolved measurements with wideband transceivers. VNA compatibility is provided by IQ splitting/combining via 90° hybrid couplers and an RF switch for polarization selection. The picture shows the 20 to 50 GHz variant with RFspin QRH50E antenna. A similar converter pair is available for 5 to 20 GHz with RFspin QRH20E antenna. See Table II for technical details.

We designed and assembled two pairs of quadrature frequency converters in coaxial technology: One up-converter (Tx) and one down-converter (Rx) each for the frequency ranges from 5 to 20 GHz and from 18 to 50 GHz. All converters use dual linearly polarized antennas and fully parallel microwave branches for both polarizations, requiring four ADC/DAC ports per converter. Technical details are summarized in Table II. The components are integrated into a shielded case with microwave absorbers magnetically mounted on the front and a flange compatible with BIRA, see Fig. 5. Phase-aligned operation of Tx and Rx is ensured by local oscillator (LO) sharing: Within the BIRA setup, the LO is distributed via RFoF from a common signal generator (Keysight EXG N5173B).

The quadrature probes support VNAs through analog signal adapters: The IQ channels are externally combined via 90° hybrid couplers and polarization selection is carried out via microwave switches that are controlled remotely with GPIO signals. The integrated RF cables (cf. Sec. IV-A) then route the resulting single IF signal between each probe and the VNA.

E. Waveguide Converters

Targeting frequencies above 67 GHz requires switching from coaxial to waveguide components. Three pairs of converters are available for the waveguide bands WR-12 (60 to 90 GHz), WR-6.5 (110 to 170 GHz), and WR-4.3 (170 to 260 GHz), see Fig. 6. Within these frequency ranges, individual bands can be selected by exchanging band-pass filters. The trade-off between antenna directivity and angular field-of-view is addressed by multiple antenna pairs. All parameters are documented in Table II. All waveguide converters are implemented single-polarized. Dual-polarized measurements

TABLE II
PARAMETERS OF BIRA MICROWAVE PROBES

	non-converting RF probe	IQ converter	IQ converter	WR-12 converter	WR-6.5 converter	WR-4.3 converter
frequency range	0.7...20 GHz	5...20 GHz	20...50 GHz	60...90 GHz	110...170 GHz	170...260 GHz
RF filters	–	–	–	76...81 GHz 60...90 GHz 70...90 GHz	140...148 GHz 110...140 GHz 140...170 GHz	200...260 GHz
IF range	cf. VNA and transceivers	0...6 GHz	0...23 GHz	...12 GHz	...17 GHz	...26 GHz
LO range	(via RFoF) ...30 GHz	5...20 GHz	9...25 GHz	15...22 GHz	18.3...28.3 GHz	14.2...21.6 GHz
Tx $P_{out,dB}$	25 dBm	16 dBm	10 dBm	6 dBm	1 dBm	-3 dBm
Tx $P_{in,dB}$	7 dBm	-2 dBm	-2 dBm	-20 dBm	-20 dBm	-20 dBm
Tx converter gain	(RF AMP) 38 dB	9 dB	12 dB	26 dB	21 dB	17 dB
Rx noise figure	(LNA) 3...4 dB	7 dB	5 dB	6...7 dB	7...8 dB	8...9 dB
Rx converter gain	(LNA) 30 dB	0 dB	12 dB	38...40 dB	33...37 dB	50...55 dB
Rx $P_{in,dB}$ @LNA	-15 dBm	-1 dBm	-24 dBm	-15...-12 dBm	-22...-18 dBm	-29...-25 dBm
polarization selection	dual, linear RF switch	dual, linear parallel (2×IQ pair)	dual, linear parallel (2×IQ pair)	single, linear mechanical rotation	single, linear mechanical rotation	single, linear mechanical rotation
antennas	Schwarzbeck CTIA 0710 RFspin QRH20E	RFspin QRH20E	RFspin QRH50E	25 dBi, 9° 20 dBi, 14° 15 dBi, 30° 10 dBi, 55°	25 dBi, 9° 20 dBi, 17° 15 dBi, 33°	25 dBi, 10°

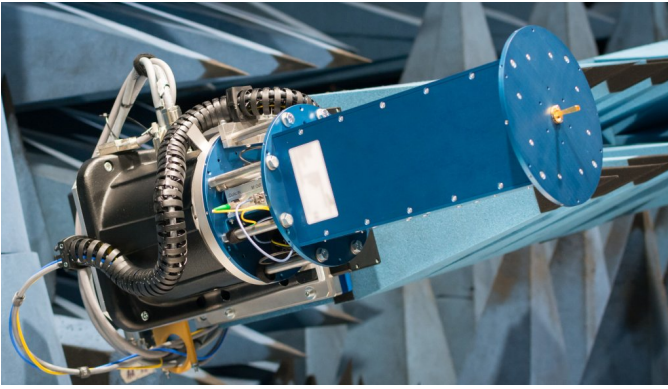


Fig. 6. Frequency converter, implemented in waveguide technology. Here, the frontal absorbers have been removed to make the minuscule horn antenna visible. LO signals are distributed optically via an RFoF module that is stacked between the BIRA flange and the frequency converter case. The photograph depicts the WR-6.5 waveguide band variant (110 to 170 GHz). Similar converters are available as well for WR-12 (60 to 90 GHz) and WR-4.3 (170 to 260 GHz). See Table II for technical details.

are realized by remote-controlled mechanical rotation of the probes. As with the IQ converters, phase-aligned operation is ensured by LO distribution via RFoF and by applying LO multiplication. Hardware integration and supply of the waveguide converters was provided by the contractor *bsw TestSystems & Consulting AG*.

V. SOFTWARE

The operation of the eight mechanical BIRA axes is not straightforward. Firstly, its machine coordinates differ from the bistatic angles φ_i , θ_i , φ_o , and θ_o of both probes with respect to the DUT. The mapping from bistatic angles to machine coordinates is not unique. Secondly, collisions, although prevented by firmware, are hypothetically possible, due to that fact that both gantry positioners move along the same sphere around the focal point. This necessitates careful planning of measurement trajectories, i.e., consecutive lists of positioner waypoints, to ensure uninterrupted operation. The trajectories

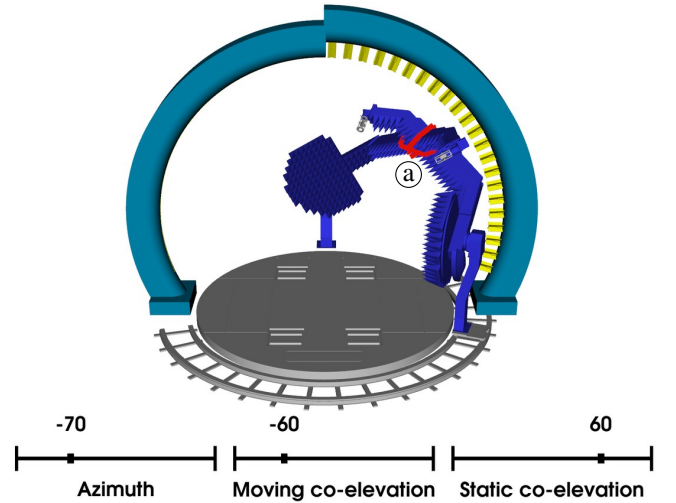


Fig. 7. Screenshot of BIRA's digital twin with interactive GUI enabled and both gantries colliding. Bounding boxes with 10 cm safety clearance are used for collision detection but not rendered. Only bounding box polygon intersections, i.e., likely collisions, are drawn in red \textcircled{a} .

must pre-emptively circumnavigate gantry collisions while also minimizing the extent of detours incurred by this process.

Our BIRA software suite comprises two primary components: A mechanically exact digital twin and a hardware abstraction layer combined with a generic API.

A. Interactive Digital Twin

We implemented the digital twin using the Python programming language and the Visualization Toolkit (VTK) computer graphics library. The twin relies on the actual computer aided design (CAD) models of BIRA to implement its geometrically exact replica. Additionally, a simplified bounding box is used for collision detection with a safety clearance of 10 cm.

The digital twin includes an optional, interactive graphical user interface (GUI) (see Fig. 7). The GUI visualizes the machine coordinate system, which facilitates system familiarization for first-time users and accelerates measurement trajec-

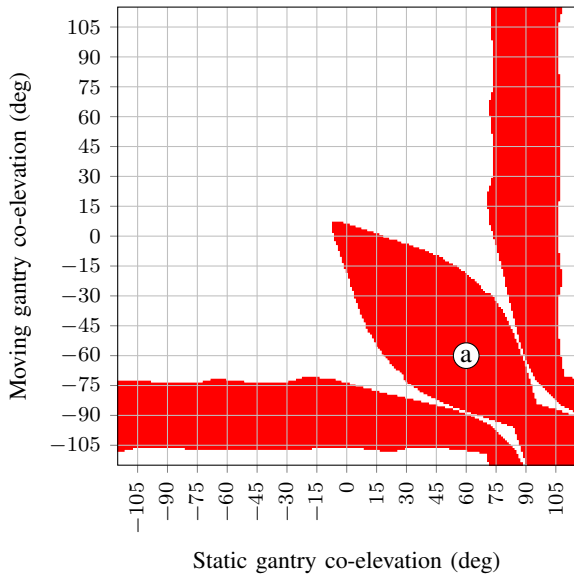


Fig. 8. 2-dimensional slice of collision table generated by digital twin for the machine coordinate azimuth angle -70° . Red areas denote angle combinations where bounding boxes collide. The gantry positions of the collision rendered in Fig. 7 are marked by \textcircled{a} .

tory planning significantly. We also employ the GUI for safe interactive control of BIRA by visualization of movements prior to execution.

The digital twin is essential for mechanical safety. Being realized as a multi-purpose library with a flexible API, we also use it to compute a collision table containing all possible permutations of the three main mechanical axes of BIRA: Moving gantry azimuth and co-elevation as well as static gantry co-elevation. The remaining axes' range of motion precludes these axes from any contribution to possible collisions. The table contains approximately 10 million entries at 1° angular resolution, see Fig. 8 for an exemplary section of the table. The simplified bounding boxes used to compute intersections result in a short half-hour computation time, facilitating generation and use of collision tables for non-standard probes or even very large DUTs. A default table for cylindrical probes as depicted in Sec. IV is used by the firmware and possibly custom tables are used by the software to implement failsafe, multi-layered collision prevention.

B. Hardware Abstraction Layer and Application Programming Interface (API)

The primary design goal of BIRA was universal usability, requiring a generic API not limited to specific measurement types. This user-facing API must satisfy the following requirements in the order of priority: Mechanical safety, efficiency, and user-friendliness. All requirements rule out granting these users direct access to the positioner hardware. Instead, we opted for a safety enforcing yet straightforward abstraction layer: A trajectory and parameter file in JavaScript Object Notation (JSON). It provides a list of consecutive positions for all eight axes. JSON is a language-independent data interchange format that is natively supported by many programming languages, e.g., MATLAB and R.

The remainder of the software was implemented in Python. We developed a kinematic model of all eight axes, which incorporates their velocity-, acceleration-, and jerk-limited motion. This model enables offline verification of user-supplied trajectories: For each movement between subsequent trajectory steps, the kinematic model provides the fine-grained intermediate positions of all axes, which are checked against the collision table computed by the digital twin. We also use the kinematic model to predict exact measurement duration and to check trajectory efficiency, e.g., to identify detours.

The actual measurement software interfacing the positioner hardware is strictly isolated from the users for safety reasons. Only operators, i.e., trained, experienced, and subsequently authorized staff members, initiate measurements using JSON trajectory files that have passed offline verification. These operators also select additional axis motion parameters, i.e., velocity, acceleration, and deceleration, based on user requirements, simplifying the users' trajectory preparation from 29 to only eight parameters. This approach ensures safety and efficiency. Verified trajectories can be used for long-term, unattended measurements over night or weekends.

Our measurement software interfaces the turntable, the gantry positioners, and the microwave measurement devices via an Ethernet local area network. The involved industrial motor control interfaces have response latencies around 100 ms. With four bistatic angles and thus four primary degrees of freedom, typical measurement times range from several hours up to multiple days. This implies that even minor efficiency gains can result in significant time savings. Therefore, we implemented fully parallelized network remote control using Python's *asyncio* library and asynchronous coroutines. We batch movement commands for multiple axes into single network requests and optimize for successful command execution by deferring error checks until after all movement commands were issued. This way, we achieve a total remote control overhead of only 100 ms. In contrast, multiple sequential network requests would add up request latencies, accumulating up to several hours for long-term measurements.

Like BIRA itself, our software also supports arbitrary applications. This requires the integration of custom user code into the measurement software program flow. Obviously, user-provided program code and data must remain strictly isolated from the positioner hardware for safety reasons. We realized this through a restricted callback API. For stepped measurements, our software calls a user-provided function after all axes have come to standstill at their respective target position. For continuously moving measurements, our software runs an asynchronous user-provided coroutine in parallel to continuously orchestrating all motions. The user code has read-only access to all states, e.g., current position and velocity, i.e., cannot issue any commands. To facilitate the development of user code, the measurement software can run fully offline without hardware access, partially simulating positioner behavior. However, default implementations for VNA and SDR measurements are available and can be used without modification for most measurement applications.

VI. SUMMARY

In this paper, we introduced our “Bistatic Radar” (BIRA) measurement system, which extends the Virtual Road – Simulation and Test Area (VISTA) with two universal mechanical positioners. Together with DUT rotation by the turntable, independent illumination and observation angles of both more than a hemisphere (0 to 360° azimuth, 0 to 114° co-elevation) are realized with sub-millimeter accuracy. This comprehensive upgrade was inaugurated in 2023 and addresses the requirements of research for 6G and beyond in the upcoming decades [22]–[29]. Although motivated by and named after bistatic radar, i.e., ISAC, our BIRA system is entirely use-case agnostic and includes a variety of features useful for 3D antenna pattern measurements up to the sub-THz frequency range.

BIRA is a modular spherical positioning system for DUTs up to the size of a passenger car. Either positioner can be installed and used independently. A universal probe flange, power supply, integrated microwave cabling and LO distribution, and generic low-level API support almost arbitrary payloads and ensure future upgradability. A digital twin ensures the safe operation of the positioners, facilitates measurement planning for researchers, and accelerates software development.

Currently available microwave probes include coaxial frequency converters for parallel, dual-polarized measurements up to 50 GHz and linearly polarized waveguide converters for almost continuous signal coverage up to 260 GHz. All probes are baseband agnostic and compatible with a monolithic VNA as well as distributed SDR transceivers.

BIRA is a bistatic reflectivity measurement facility suitable for unrestricted ISAC research. It is one of only two installations with at least four spherical degrees of freedom, which is the minimum required for fully bistatic reflectivity measurements. Secondly and more importantly, BIRA employs distributed SDR transceivers, while other installations use VNAs [8]–[16] with theoretically zero instantaneous bandwidth, restricting their applicability to the reflectivity of stationary objects. In contrast, the instantaneous bandwidth of the SDR transceivers (up to 4 GHz) enables dynamic ISAC measurements with superior range resolution of up to 3.75 cm. BIRA provides novel and highly relevant experimental access to the bistatic radar reflectivity of extended objects and antenna characterization up to the sub-THz range. Selected examples of both tasks will be presented in a forthcoming version of this paper. With these features, BIRA presents a unique asset of the Thuringian Center of Innovation in Mobility.

REFERENCES

- [1] M. A. Hein, C. Bornkessel, W. Kotterman, C. Schneider, R. K. Sharma, F. Wollenschläger, R. S. Thomä, G. Del Galdo, and M. Landmann, “Emulation of virtual radio environments for realistic end-to-end testing for intelligent traffic systems,” in *2015 IEEE MTT-S International Conference on Microwaves for Intelligent Mobility (ICMIM)*, 2015, pp. 1–4, doi: 10.1109/ICMIM.2015.7117934.
- [2] B. Altinel, F. Wollenschläger, and M. A. Hein, “Interference Tests of ITS-G5 Vehicle-to-Vehicle Communication Networks with Virtual Drive Tests,” in *2019 IEEE International Conference on Connected Vehicles and Expo (ICCVE)*, 2019, pp. 1–5, doi: 10.1109/ICCVE45908.2019.8965140.
- [3] P. Berlt, C. Bornkessel, and M. A. Hein, “Accurate 3D Phase Recovery of Automotive Antennas Through LTE Power Measurements on A Cylindrical Surface,” in *2020 14th European Conference on Antennas and Propagation (EuCAP)*, 2020, pp. 1–5, doi: 10.23919/EuCAP48036.2020.9135443.
- [4] S. B. J. Gowdu, M. E. Asghar, R. Stephan, M. A. Hein, J. Nagel, and F. Baumgärtner, “System architecture for installed-performance testing of automotive radars over-the-air,” in *2018 IEEE MTT-S International Conference on Microwaves for Intelligent Mobility (ICMIM)*, 2018, pp. 1–4, doi: 10.1109/ICMIM.2018.8443490.
- [5] S. N. Hasnain, A. Khakimov, U. Stehr, and M. A. Hein, “Emulation of Realistic Satellite Constellations for GNSS Receiver Testing in Virtual Environment,” in *2023 17th European Conference on Antennas and Propagation (EuCAP)*, 2023, pp. 1–5, doi: 10.23919/EuCAP57121.2023.10133419.
- [6] A. Schwind, R. Stephan, and M. A. Hein, “Simulations and Measurements of the Bistatic Radar Cross Section of Vulnerable Road Users between 2 GHz and 6 GHz,” in *2018 IEEE MTT-S International Conference on Microwaves for Intelligent Mobility (ICMIM)*, 2018, pp. 1–4, doi: 10.1109/ICMIM.2018.8443498.
- [7] A. Schwind, M. Döbereiner, C. Andrich, P. Wendland, G. Del Galdo, G. Schaefer, R. S. Thomä, and M. A. Hein, “Bi-static delay-doppler reference for cooperative passive vehicle-to-x radar applications,” *IET Microwaves, Antennas & Propagation*, vol. 14, no. 14, pp. 1749–1757, 2020, doi: 10.1049/iet-map.2019.0991.
- [8] D. Escot, D. Poyatos, J. A. Aguilar, I. Montiel, I. González, and F. Saez de Adana, “Indoor 3D Full Polarimetric Bistatic Spherical Facility for Electromagnetic Tests,” *IEEE Antennas and Propagation Magazine*, vol. 52, no. 4, pp. 112–118, 2010, doi: 10.1109/MAP.2010.5638248.
- [9] P. López-Rodríguez, O. Hernán-Vega, D. Poyatos-Martínez, and D. Escot-Bocanegra, “BIANCHIA: A spherical indoor facility for bistatic electromagnetic tests,” in *AMTA 2016 Proceedings*, 2016, pp. 1–6, doi: 10.1109/AMTAP.2016.7806285.
- [10] “BIANCHIA (Bistatic ANechoic CHamber),” <https://triasrnd.com//446-bianchia-bistatic-anechoic-chamber>, accessed: 2024-06-03.
- [11] Y. Chevalier, P. Minvielle, F. Degery, and P. Berisset, “Indoor Spherical 3-D RCS Near-Field Facility,” in *29th Annual Symposium of the Antenna Measurement Techniques Association (AMTA)*, 2007.
- [12] S. Bellez, H. Roussel, C. Dahon, J. C. Castelli, and A. Chery, “Full Polarimetric Bistatic Radar Imaging Experiments on Sets of Dielectric Cylinders Above a Conductive Circular Plate,” *IEEE Transactions on Geoscience and Remote Sensing*, vol. 51, no. 7, pp. 4164–4176, 2013, doi: 10.1109/TGRS.2012.2227264.
- [13] A. J. Sieber, “The European Microwave Signature Laboratory,” in *IGARSS ’92 International Geoscience and Remote Sensing Symposium*, 1992, doi: 10.1109/IGARSS.1992.578382.
- [14] “European Microwave Signature Laboratory,” https://joint-research-centre.ec.europa.eu/laboratories-z/european-microwave-signature-laboratory-and-eu-gnss-simulation-and-receiver-testing-facilities_en, accessed: 2024-06-03.
- [15] W. Tian, Y. Shao, Z. Liu, Q. Wei, Z. Tang, and C. Ni, “A Full-Parameters Microwave Properties Measurement System of 20m Diameter Anechoic Chamber,” in *IEEE International Geoscience and Remote Sensing Symposium IGARSS*, 2021, doi: 10.1109/IGARSS47720.2021.9554412.
- [16] “The anechoic chamber in LAMP,” <http://www.dasa.net.cn/h-col-108.html>, accessed: 2024-06-03.
- [17] F. Bevilacqua, F. D’Agostino, F. Ferrara, C. Gennarelli, R. Guerriero, and M. Migliozi, “A near to far-field transformation from plane-polar near-field measurements affected by 3-d probe positioning errors,” in *2023 17th European Conference on Antennas and Propagation (EuCAP)*, 2023, pp. 1–5, doi: 10.23919/EuCAP57121.2023.10133532.
- [18] S. Giehl, C. Andrich, M. Schubert, M. Engelhardt, and A. Ihlow, “Receiver Bandwidth Extension Beyond Nyquist Using Channel Bonding,” in *2023 17th European Conference on Antennas and Propagation (EuCAP)*, 2023, pp. 1–5, doi: 10.23919/EuCAP57121.2023.10133262.
- [19] H. C. Alves Costa, S. J. Myint, C. Andrich, S. W. Giehl, C. Schneider, and R. S. Thomä, “Modelling Micro-Doppler Signature of Drone Propellers in Distributed ISAC,” in *2024 IEEE Radar Conference (RadarConf24)*, 2024, pp. 1–6, doi: 10.1109/RadarConf2458775.2024.10548468.
- [20] —, “Bistatic Reflectivity and Micro-Doppler Signatures of Drones for Integrated Communication and Sensing,” in *2024 25th International Radar Symposium (IRS)*, 2024, pp. 1–6, doi: 10.48550/arXiv.2401.14448, accepted for publication.
- [21] M. Engelhardt, S. Giehl, M. Schubert, A. Ihlow, C. Schneider, A. Ebert, M. Landmann, G. Del Galdo, and C. Andrich, “Accelerating Innovation

- in 6G Research: Real-Time Capable SDR System Architecture for Rapid Prototyping,” 2024, arXiv:2402.06520 [eess.SP].
- [22] P. Rosemann, S. Partani, M. Miranda, J. Mähm, M. Karrenbauer, W. Meli, R. Hernangomez, M. Lübke, J. Kochems, S. Köpsel, A. Aziz-Koch, J. Beuster, O. Blume, N. Franchi, R. Thomä, S. Stanczak, and H. D. Schotten, “Enabling Mobility-Oriented JCAS in 6G Networks: An Architecture Proposal,” in *4th IEEE International Symposium on Joint Communication and Sensing*, 2024, doi: 10.48550/arXiv.2311.11623.
- [23] “Future technology trends of terrestrial International Mobile Telecommunications systems towards 2030 and beyond,” International Telecommunication Union, Rep. ITU-R M.2516-0, 2022. [Online]. Available: https://www.itu.int/dms_pub/itu-r/opb/rep/R-REP-M.2516-2022-PDF-E.pdf
- [24] “Framework and overall objectives of the future development of IMT for 2030 and beyond,” International Telecommunication Union, Rec. ITU-R M.2160-0, 2023. [Online]. Available: https://www.itu.int/dms_pubrec/itu-r/rec/m/R-REC-M.2160-0-202311-I!!PDF-E.pdf
- [25] “Integrated Sensing and Communication,” 3GPP, SP-230750, 2023. [Online]. Available: https://www.3gpp.org/ftp/Information/WI_Sheet/SP-230750.zip
- [26] “Feasibility Study on Integrated Sensing and Communication,” 3GPP, TR 22.837 V19.4.0, 2024. [Online]. Available: https://www.3gpp.org/ftp/Specs/archive/22_series/22.837/22837-j40.zip
- [27] “Study on channel modelling for Integrated Sensing and Communication (ISAC) for NR,” 3GPP, RP-240799, 2024. [Online]. Available: https://www.3gpp.org/ftp/Information/WI_Sheet/RP-240799.zip
- [28] “The European view on 6G use cases,” 6G SNS-ICE, SWS-240018, *3GPP Stage 1 Workshop on IMT2030 Use Cases*, 2024. [Online]. Available: https://www.3gpp.org/ftp/workshop/2024-05-08_3GPP_Stage1_IMT2030_UC_WS/Docs/SWS-240018.zip
- [29] “NGA Vision for 6G,” NextG Alliance, SWS-240017, *3GPP Stage 1 Workshop on IMT2030 Use Cases*, 2024. [Online]. Available: https://www.3gpp.org/ftp/workshop/2024-05-08_3GPP_Stage1_IMT2030_UC_WS/Docs/SWS-240017.zip